Dalton Transactions

Accepted Manuscript

ROYAL SOCIETY OF CHEMISTRY

www.rsc.org/dalton

Cite this: DOI: 10.1039/c0xx00000x

www.rsc.org/xxxxxx

ARTICLE TYPE

Femtosecond spectroscopy and TD-DFT calculations of $CuCl_4^{2-}$ excited states

Elena N. Golubeva[a], Ekaterina M. Zubanova[a,b], Mikhail Ya. Melnikov[a], Fedor E. Gostev[b], Ivan V. Shelaev[b] and Victor A. Nadtochenko[a,b,c]

Received (in XXX, XXX) Xth XXXXXXXXX 20XX, Accepted Xth XXXXXXXXX 20XX
DOI: 10.1039/b000000x

Photoinduced processes of tetrahexyl ammonium tetrachlorocuprate $[(C_6H_{13})_4N]_2Cu^{II}Cl_4$ in chloro-organic solvents were investigated by steady state photolysis and femtosecond transient absorption spectroscopy. The quantum yield of photoreduction of $CuCl_4^{2-}$ was estimated as about 1 %; the process resulted in the formation of the copper(I) chlorocomplex $Cu^{I}Cl_3^{2-}$ and a chlorine atom. Femtosecond laser photolysis with a 422 nm, 40 fs pulse revealed a three-exponential decay of the LMCT excited state of $[(C_6H_{13})_4N]_2CuCl_4$. A global fitting SVD analysis of the femtosecond transient spectra suggested three relaxation times ~400 fs, ~ 1.4 ps and ~5.8 ps. Oscillations in transient absorption kinetic traces were documented for $CuCl_4^{2-}$ solutions in 2-chlorobutane. The oscillation Fourier transform analysis and Linear Predictive Singular Value Decomposition revealed peaks at 283 cm^{-1} (damping time ~ 600 fs) and 181 cm^{-1} (damping time ~ 400 fs) . These peaks can be tentatively attributed to ν_s(Cu-Cl) symmetric stretching frequency A_1 and T_2 reflecting excited state vibrational coherence. Quantum chemical calculations suggest a possible scheme of relaxation pathways in $CuCl_4^{2-}$. The observed transient excited state absorption bands agree semiquantitatively with calculated transition bands of $CuCl_4^{2-}$.

.

Introduction

Phototransformations of coordination compounds are perspective model reactions for studying mechanisms of many biological and chemical processes[1-3]. Thus, chlorocuprate $CuCl_4^{2-}$ is considered as an unsophisticated analogue of more complicated photosystems, e.g. blue copper proteins.[4] The composition of products of photochemical reactions of coordination compounds always depends on the electronic structure of excited states. Thus, an excitation to the ligand-metal charge transfer (LMCT) absorption band of copper(II) chloro complexes usually leads to their photoreduction forming copper(I) complexes. Two mechanisms of photoreduction of chlorocuprates have been proposed. The first one includes *inner-sphere* electron transfer from chlorine to copper and leads to the formation of a chlorine atom and copper(I) complexes in a primary photochemical reaction[5]. This mechanism was proposed for systems such as $CuCl(MeOH)_5^{+}$[6,7], copper chlorides:polyethylene oxide[8], or $CuCl_2$ in different organic solvents[5]. In these systems the formation of chlorine atoms was determined by registering the characteristic CT band of complexes between $Cl^{\bullet}$ and a solvent molecule or by detecting organic radicals as products of $Cl^{\bullet}$ interaction with solvent or other reagents[6,7]. Another mechanism proposed involves *outer-sphere* electron transfer from a solvent molecule such as dmf, EtOH etc., to excited $CuCl_4^{2-}$ and leads to the formation of radicals by detaching of hydrogen from solvent molecules[9,10]. Neither of these mechanisms exclude the possibility of secondary thermal reactions of organic radicals with copper(I) complexes, which may lead to the formation of organocuprates(II) (copper complexes with a Cu(II)-C σ-bond). Such complexes were obtained under steady-state photolysis of copper chlorides in different solvents and it was proved by a combination of experimental (ESR, UV-Vis spectroscopy)[9-13]and theoretical (DFT calculations)[14,15] methods. Cu(I) complexes form adducts with a wide variety of alkyl-type radicals, such as $^{\bullet}CH_3$[16-18], $\bullet CR^1R^2OH$ and $\bullet CH_2CR^1R^2OH$[19], poly(acrylates) derivatives[20,21]. Organocuprates(II) have shown to have short lifetimes (10^{-2} - 10^{-6} s) [15-17] at ambient conditions and decay during few minutes in frozen matrices at 100-110 K[12,15]. Nevertheless, they are considered to be intermediates of catalytic radical reactions[22], such as polyhalohydrocarbon addition to alkenes[23], living radical polymerization[24], cyclization[2], C-Cl bond metathesis[25], etc.

In the present paper femtosecond spectroscopy of tetrahexyl ammonium tetrachlorocuprate $[(C_6H_{13})_4N]_2CuCl_4$ in chloro-organic solvents combined with quantum-chemical calculations of the electronic terms of excited states were performed. The purpose of this study was to elucidate the mechanism of $CuCl_4^{2-}$ phototransformations, and first of all, to resolve the ultrafast dynamics of the excited states and the possibility of formation of chloroorganocuprates at ambient conditions.

Methodology

Experimental details

Reagents. Anhydrous copper(II) chloride was obtained by azeotropic drying of the hydrate $CuCl_2•2H_2O$ with benzene and dried under vacuum at 10^{-3} torr. Tetrahexylammonium chloride $(C_6H_{13})_4N^+Cl^-$ from Sigma-Aldrich was degassed at 10^{-3} Torr. 2-Chlorobutane from Sigma-Aldrich was distilled over phosphorous pentoxide. Chlorobenzene was distilled at 10 Torr over phosphorous pentoxide. The solutions of $[(C_6H_{13})_4N]_2CuCl_4$ were prepared by dissolving $(C_6H_{13})_4N^+Cl^-$ and $CuCl_2$ in the solvents, followed by serial dilution. The concentration of $CuCl_4^{2-}$ in chlorobenzene was varied from 1.1×10^{-2} to 1.6×10^{-2} mol l^{-1}. The concentration of $CuCl_4^{2-}$ in 2-chlorobutane was equal to 5×10^{-3} mol l^{-1}. In order to prevent the formation of bi- and polynuclear copper chlorides, an excess of chloride ions was added with the ratio of $[Cl^-]/[Cu^{2+}]$ being equal to eight. The

composition of the solutions was monitored by steady-state absorption spectroscopy.

Steady-state photolysis. The procedure of preparing samples for steady photolysis was described earlier[13]. The photolysis of the solutions of $[(C_6H_{13})_4N]_2CuCl_4$ in chlorobenzene was carried out at 293 K with light of a DRSh-250 high-pressure mercury lamp using a glass filter for selecting the line at 405 nm (T_{max} = 27%, $\Delta\nu_{½}$ = 2400 cm^{-1}). The concentration of $CuCl_4^{2-}$ during the photolysis was estimated by EPR spectroscopy using a previously reported method[13]. The series of EPR spectra at different points during the photolysis were recorded at 77 K on a Varian-E3 X-band spectrometer (100 kHz magnetic field modulation). The concentration of $CuCl_4^{2-}$ was calculated from full double integration of EPR spectra according to Vorobiev et al[26]. The dependence of the $CuCl_4^{2-}$ concentration on the doze of absorbed light was calculated and plotted as described earlier[13].

Femtosecond laser photolysis setup. Transient absorption spectra were measured by the femtosecond pump/supercontinuum probe setup. The output of a Ti:sapphire oscillator (800 nm, 80 MHz, 80 fs, «Tsunami», «Spectra-Physics», USA) was amplified by a regenerative amplifier system («Spitfire», «Spectra-Physics», USA) at the repetion rate of 1 kHz as described earlier[27]. The amplified pulses were split into two beams. One of the beams was directed into a non-collinearly phase-matched optical parametric amplifier. Its output, centered at 710 nm, was compressed by a pair of quartz prisms. The Gauss pulse of about 40 fs at 422 nm with the bandwith of ~20 nm (full width at half-maximum) was used as a pump (see SI). The second beam was focused onto a thin quartz cell with H_2O to generate supercontinuum probe pulses. The pump and probe pulses were time-delayed with respect to each other using a computer-controlled delay stage. They were then attenuated, recombined, and focused onto the sample cell. The pump and probe light spots had the diameters of 300 and 120 μm, respectively. The pump pulse energy was attenuated at 120 nJ to get optimal excitation on the linear part of the light curve. Experiments were carried out at 278 K in a 0.5 mm path length optical flow cell. Frequency control of laser pulses was achieved by regular device synchronization and control amplifier SDG II Spitfire 9132, manufactured by Spectra-physics (USA). The device allowed to change the pulse repetition frequency of the amplifier output from 0 to 1000 Hz.

The pump pulse operation frequency was 50 Hz, which is sufficiently low to exclude permanent bleaching of the sample due to photochemical processes in the sample. Together with the operation frequency, the circulation rate in the flow cell was fast enough to avoid multiple excitation of the same sample volume. The relative polarization of pump and probe beams were adjusted to 54.7° (magic angle) or in parallel and perpendicular polarizations, where indicated. After the sample, the supercontinuum was dispersed by a polychromator («Acton SP-300») and detected by a CCD camera («Roper Scientific SPEC-10»). Transient spectra of absorbance changes ΔA (t, λ) were recorded over the range of 400–740 nm. Because the supercontinuum is chirped, a time correction must be applied to the measured kinetic trace at every probe wavelength. For this purpose we measured the nonresonant signal from the pure solvent[28]..

Computational details

All quantum-chemical calculations were performed at the level of unrestricted density functional theory (DFT) using the quantum-chemical program package ORCA 2.9.1[29]. The hybrid exchange-correlation functional B(38HF)P86[30] was applied for all calculations. This functional was calibrated by Solomon et al. corresponding to the ground-state spin density on the Cu-atom of the tetrachlorocuprate anion which is a well-established method for modeling electronic and magnetic molecular properties of Cu(II) compounds[14,15]. The basis set aug-TZVPP[31,32] with diffuse and polarization functions was used for Cu and Cl atoms, while the split-valence basis sets SVP[31] and SV[31] were used for C, H, and N atoms of tetramethylammonium and tetrapropylammonium counter-ions, respectively. The COSMO (COnductor-like Screening MOdel)[33] for accounting 2-chlorobutane as solvent (dielectric constant ε = 8.136, refractive index n = 1.396) was employed in all calculations besides those for excited state optimization since it was not implemented in ORCA software. Tetramethylammonium tetrachlorocuprate $[(CH_3)_4N^+]_2[CuCl_4^{2-}]$ with short alkyl chains was chosen as model compound for the electronic terms calculations making the calculations cheaper. Tetrapropylammonium tetrachlorocuprate $[(C_3H_7)_4N^+]_2[CuCl_4^{2-}]$ was chosen for geometry estimation of the sixth electronic excited state as a model which is closer to the experimentally investigated species. The full geometry optimization followed by fundamental frequencies calculation of $[(C_3H_7)_4N^+]_2[CuCl_4^{2-}]$, $[(C_3H_7)_4N^+]_2[CuCl_3^{2-}]$, $[(CH_3)_4N^+]_2[CuCl_4^{2-}]$, $(CH_3)_4N^+[CuCl_3^-]$, $[(CH_3)_4N^+]_2[CuCl_3^{2-}]$, $(CH_3)_4N^+Cl^-$ was performed; no imaginary frequencies were obtained testifying that minima, not saddle points on potential energy surfaces, were found. A relaxed scan along the Cu-Cl bond in $[(CH_3)_4N^+]_2[CuCl_4^{2-}]$ from 2.1 to 4 Å with 0.05-0.2 Å step sizes was carried out. The time-dependent DFT calculations of the ten first electronic excited states were performed for each point from the bond scan of the ground state, and the ground and excited electronic terms were plotted. Optimization of the sixth electronic excited state of $[(C_3H_7)_4N^+]_2[CuCl_4^{2-}]$ was performed within the scope of the TDDFT approach[34] with RIJCOSX approximation[35].

Results

Steady State Photolysis

During the stationary photolysis of $[(C_6H_{13})_4N]_2CuCl_4$ solutions in chlorobenzene, the decrease of the intensity of $CuCl_4^{2-}$ EPR spectrum was observed, while the signal shape and magnetic parameters remained unchanged in all studied solutions. Dependencies of $CuCl_4^{2-}$ concentration on absorbed light dose were linear up to 90-95% of conversion. The quantum yield was independent on the initial concentration of tetrachlorocuprate; its average value was equal to $1.4(\pm 0.2)\times 10^{-2}$. Reactive intermediates such as alkyl radicals or copper(II) organic compounds were not detected.

Femtosecond Absorption Spectra

Ultrafast time-resolved transient absorption ΔA spectra following 422 nm excitation of $CuCl_4^{2-}$ in 2-chlorobutane solution and their evolution from 100 fs to 340 ps are presented in Figure 1. In comparison with the transient absorption of the sample solution, the ΔA signal from neat 2-chlorobutane was measured under identical excitation conditions. Transient absorption spectra for the short time delay of 100 fs reveal a broad, unstructured excited-state absorption (ESA) band at wavelengths longer than 475 nm and a negative transient absorption for wavelengths shorter than 475 nm that can be tentatively attributed to a stimulated emission (SE) band of electronically excited state of $CuCl_4^{2-}$ or to a bleach (BL) band with a maximum near 450 nm due to the depletion of the ground state. The dominant feature at all times longer than 300 fs is a couple of ESA bands with two broad peaks about 500 nm and 610 nm. The peak positions are shifted to the blue side. As it can be seen from Figure 1b, the

transient absorption spectrum is transformed to one ESA band at 480 nm at a time delay of 340 ps. These features are displayed in Figure 2b with enlarged scale.

Kinetic traces for selected probe frequencies are shown in Figure 2. Because of the coherent structure and other fast changes at early times, kinetic traces are shown for time delays longer than 80 fs. Kinetic traces at short times (shown in Figure 2a) depict rise and decay components, whereas at long time delays (Figure 2b), the kinetic traces show decay. Three characteristic constants were determined by exponential and biexponential fitting of the kinetic

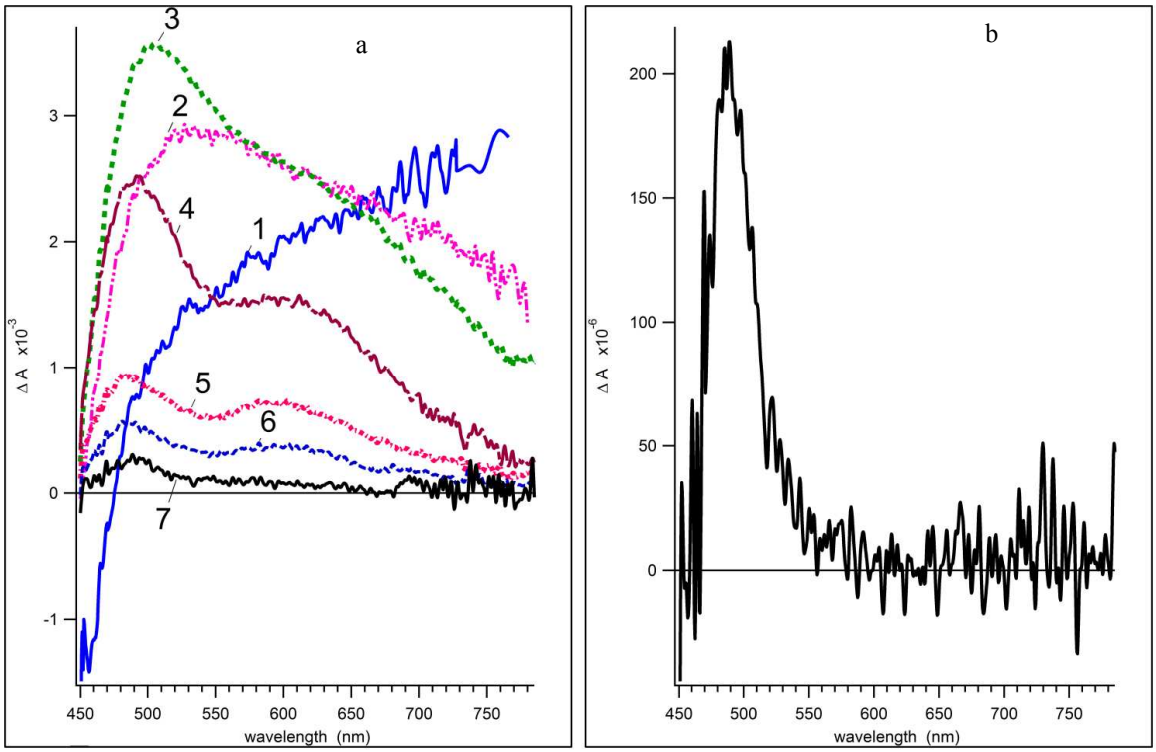

Figure 1. Transient absorption spectra of $[(C_6H_{13})_4N]_2CuCl_4$ solutions in 2-chlorobutane following 422 nm excitation : a) time delay is100 fs (1), 310 fs (2), 510 fs (3), 1.3 ps (4), 5 ps (5), 8 ps (6), 340 ps (7); b): the average spectrum obtained by averaging of spectra in the time delay window between 200 ps and 340 ps.

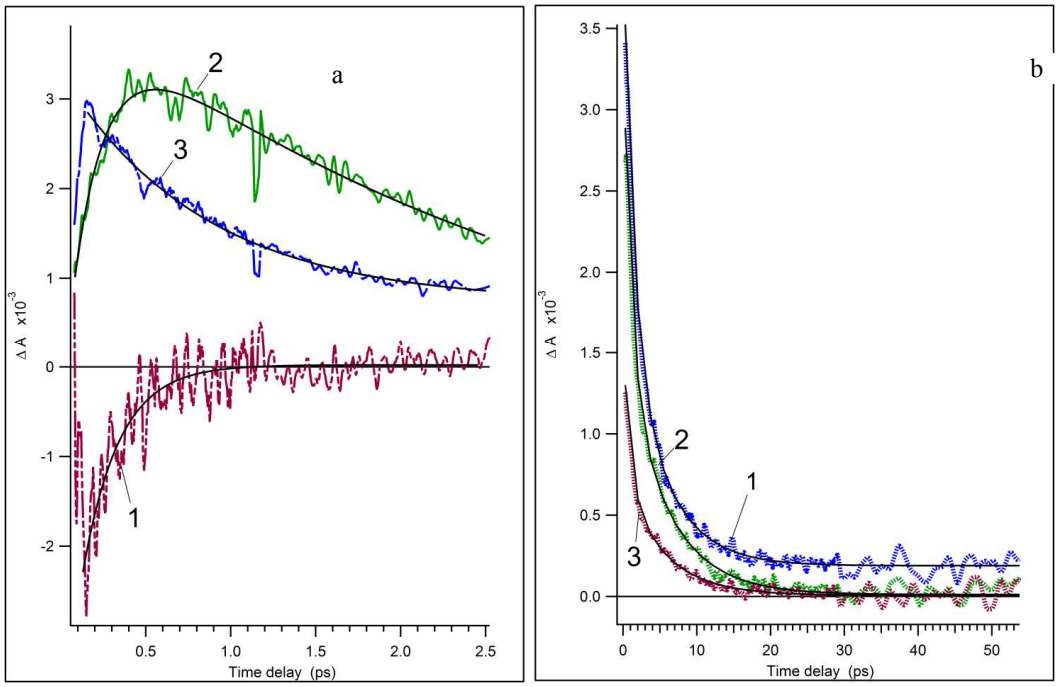

Figure 2. Kinetic traces for selected probe wavelengths. Dashed lines are experimental curves. Solid smoothed curves are fit.

Panel a) : (1) 449 nm, exponential fit was used $y_0+A_1\exp(-k_1t)$, $y_0 = (0.9 \pm 0.1)\times10^{-5}$, $A_1= (2.7 \pm 0.1)\times10^{-3}$, $k_1 = (2.5 \pm 0.3)$ 1/ps;
(2) 500 nm biexponential fit was used $y_0+A_1\times(1-\exp(-k_1 t))\times\exp(-k_2 t)$, $y0 = (4 \pm 0.5)10^{-4}$, $A_1= (4.4 \pm 0.5)\times10^{-3}$, $k_1= (3.0\pm0.2)$ 1/ps, $k_2 = (0.65 \pm0.05)$ 1/ps;
(3) 651 nm exponential fit was used $y_0+A_1\exp(-k_1t)$, $y_0=(4.4\pm0.1)\times10^{-4}$, $A_1=(2.65\pm0.14)\times10^{-3}$, $k_1=(0.7 \pm 0.07)$ 1/ps
Panel b). Biexponential fit was used $y_0+A_1\exp(-k_1t) + A_2\exp(-k_2t)$.
(1) 480 nm, $y_0= (1.9 \pm 0.0012)\times10^{-3}$, $A_1 = (1.6 \pm 0.13)\times10^{-3}$, $k_1 = 0.195 \pm 0.009$ 1/ps, $A_2 = (2.3 \pm 0.\ 11)\times10^{-3}$, $k_2 = 0.76 \pm 0.06$ 1/ps,
(2) 600 nm $y_0 = (1.1 \pm 0.08)\times10^{-5}$ $A_1= (1.5 \pm 0.05)\times10^{-3}$, $k_1 = 0.174 \pm 0.0043$ 1/ps, $A_2 = (2 \pm 0.05)10^{-3}$, $k_2= 0.98 \pm 0.06$ 1/ps,
700 nm. $y_0 = (5.8\pm 0.82)\times10^{-6}$, $A_1 = (73 \pm 4.8)10^{-5}$, $k_1= 0.18\ \pm 0.01$ 1/ps, $A_2 = (85 \pm 5.7)10^{-5}$, $k_2 = 1.0 \pm 0.15$ 1/ps.

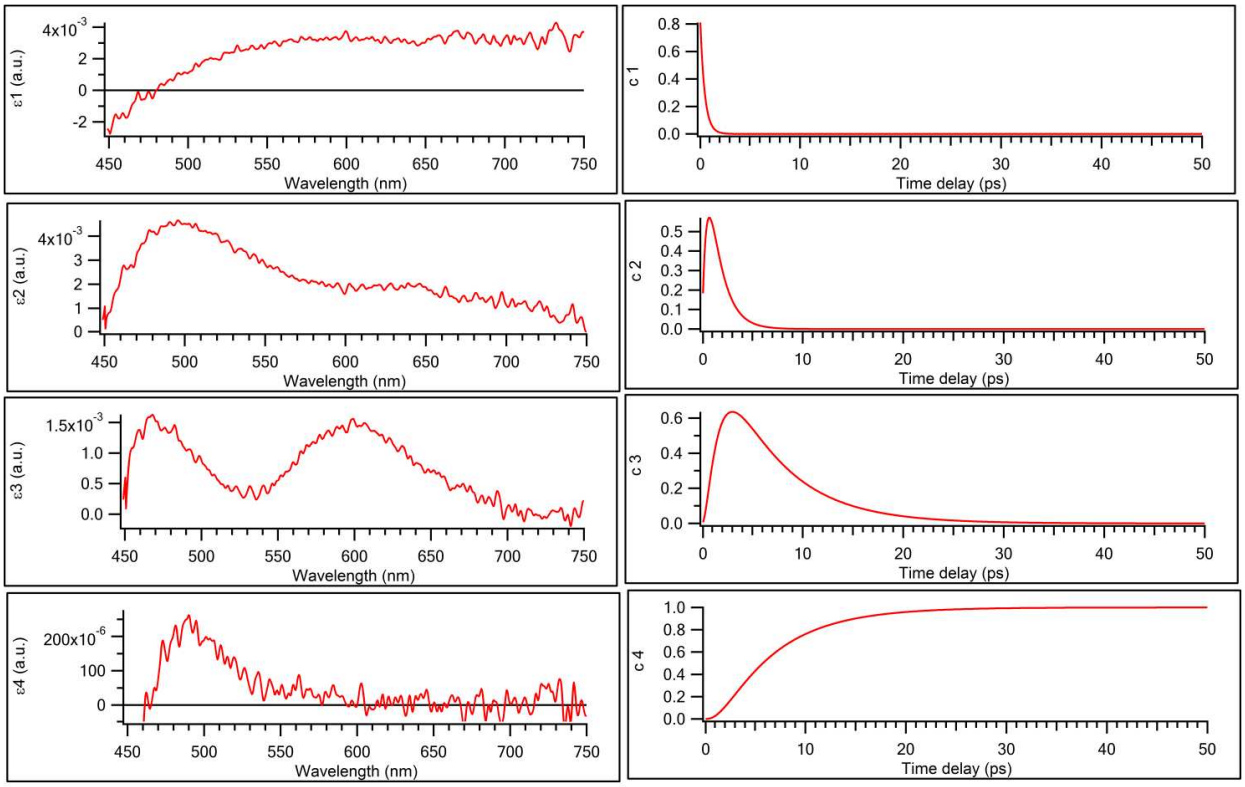

Figure 3. Species-associated spectra (left column) and species-associated kinetics (right column) for the model $c_1 \xrightarrow{k_1} c_2 \xrightarrow{k_2} c_3 \xrightarrow{k_3} c_4$ of irreversible intramolecular relaxation of the $CuCl_4^{2-}$ excited state.

traces in Figure 2. They are k_1~2.5 ps^{-1}, k_2~0.7 ps^{-1} and k_3~0.17 ps^{-1}. The observation of three rate constants suggests that four intermediate states can be taken into account for the consideration of a kinetic scheme of $CuCl_4^{2-}$ relaxation.

Kinetic traces reveal oscillations at short time delays (less than 2.5 ps) for $CuCl_4^{2-}$ in 2-chlorobutane and for pure 2-chlorobutane (Figure SI 1). The Fourier transform analysis of the oscillations and Linear Predictive Singular Value Decomposition LPSVD resolves components oscillating with vibrational frequencies of 370 cm^{-1}, 460 cm^{-1}, 517 cm^{-1}, 607 cm^{-1} for pure 2-chlorobutane. These vibrational frequencies were assigned to the torsional and low frequency bending vibrations of 2-chlorobutane, resp.,[36,37] reflecting ground state vibrational coherence[38,39]. In the solution of $CuCl_4^{2-}$ in 2-chlorobutane, additional oscillation peaks were observed at 283 cm^{-1} (damping time is ~ 600 fs) and 181 cm^{-1} (damping time is ~ 400 fs) (SI 1). These peaks can be tentatively attributed to ν_s(Cu-Cl) symmetric stretching frequency A_1 and T_2[40] reflecting excited state vibrational coherence. The damping time of the Cu-Cl oscillations are close to the relaxation time of the initial excited state 1/k1~440 fs as indicated in the paragraph below.

The intermediate states are identified by their temporal behaviour, and singular value decomposition (SVD) of $\Delta A(\lambda,t)$ is used to determine the spectra associated with these photochemical species. The induced optical density at the detection wavelengths λ_i (i = 1, M) and delay times t_j (j = 1, N) comprise a data matrix $\mathbf{A} = \Delta A(\lambda_i,t_j)$. For example, of the full spectral range we consider 711 equally spaced wavelengths from 449 to 750 nm and the delay time runs from 0.08 ps to 340 ps in 6.666 fs steps; hence, **A** has the dimension 711 x 7487. The experimental data can be presented by the following expression:

$$\Delta A(t,\lambda) = \Sigma^4_{i=1}\, \varepsilon(\lambda)_i\, c_i(t) = \mathbf{E}\,\mathbf{C},$$

where $\varepsilon(\lambda)_i$ are the spectra of individual states i and $c_i(t)$ is the population of $CuCl_4^{2-}$ intermediate states at time t.

To find rate constants as well as to reveal spectra of these states and kinetics of transitions between them, the data were analyzed using the global fit procedure according to Scheme 1. The technique of SVD of data matrix was applied to the global fit analysis. The algorithm of the global fit for femtosecond experiment is described in the literature.[41,42]

The coupled rate equations for the concentrations have the solution

$$C(t)=\begin{bmatrix}c_1(t)\\c_2(t)\\c_3(t)\\c_4(t)\end{bmatrix}=\begin{bmatrix}0 & 1 & 0 & 0\\ 0 & \frac{k_1}{-k_1+k_2} & \frac{k_1}{k_1-k_2} & 0\\ 0 & \frac{k_1k_2}{(k_1-k_2)(k_1-k_3)} & \frac{k_1k_2}{(k_1-k_2)(k_3-k_2)} & \frac{k_1k_2}{(k_1-k_3)(k_2-k_3)}\\ 1 & \frac{-k_2k_3}{(k_1-k_2)(k_1-k_3)} & \frac{k_2k_3}{(k_1-k_2)(k_3-k_2)} & -\frac{k_1k_2}{(k_1-k_3)(k_2-k_3)}\end{bmatrix}\cdot\begin{bmatrix}1\\ \exp(-k_1\cdot t)\\ \exp(-k_2\cdot t)\\ \exp(-k_3\cdot t)\end{bmatrix}=M\cdot T(t)$$

where at $t = 0$ $[f_1] = 1$ and $[f_2]=0$, $[f_3]=0$ $[f_4]=0$ was assumed.

By SVD, the data can be written as A = **U S V**^{T} where the columns of **U** represent normalized basic spectra, the rows of **V**^{T} contain their normalized dynamics, and diagonal **S** may be presumed to have the weights or singular values *Skk* > 0 arranged in descending order. Usually, just a few (L, in our case L = 4) combinations are sufficient to describe the measurement adequately. Therefore, the matrices **U**, **S**, and **V**^{T} are truncated to dimensions M x L, L x L, and L x N, respectively, after SVD. When the values for the parameters are given, the temporal functions are tabulated for the delay times *tj* to give an L x N matrix **T(t)**:

$$T(t)=\begin{bmatrix}1\\ \exp(-k_1\cdot t)\\ \exp(-k_2\cdot t)\\ \exp(-k_3\cdot t)\end{bmatrix}$$

The coefficients in **F** and the parameters k_1, k_2, k_3 in **T** must be optimized simultaneously to fit **V**^{T}≈ **F T**. The best fit was obtained with rate constants k_1=2.25 1/ps , k_2= 0.78 1/ps, k_3=0.177 1/ps. These rate constants are in accord with those rate constants determined by fitting of selected transient kinetic traces shown in Figure 2. Species-associated spectra (SAS) of intermediates **E** can be determined from

$$\mathbf{U\,S\,V^T \approx U\,S\,F\,T = (U\,S\,F\,M^{-1})\,(M\,T) = E\,C}$$

Species-associated spectra and species-associated kinetics (SAK) are shown in Figure 3.

Quantum-chemical calculations

Calculated equilibrium geometries of copper(II) and copper(I) chloride complexes are presented in Figure 4. Computed values of Cu-Cl bonds and Cl-Cu-Cl angles are in a good agreement with experimental ones[25,43] and those calculated previously[30]. The spatial symmetry of the $CuCl_4^{2-}$ anion is lower than D_{2d} and close to C_2 as a result of the influence of the counter-ion. Dependence of the symmetry of tetrachlorocuprate on the counter-ion was also confirmed by X-ray data on structure of $CuCl_4^{2-}$ anions in different media.

An electronic spectrum of $(NMe_4)_2Cu^{II}Cl_4$ calculated previously by means of TDDFT approach with correction coefficient equal to 0.91 was in good agreement with experimental data[15]. In the present paper we have applied the same procedure to compute the first ten electronic excited terms of $(NMe_4)_2Cu^{II}Cl_4$. Electronic excited terms along the Cu-Cl bond are presented in Figure 5. According to the experimental and theoretical data, excitation at 420 nm leads to LMCT transition $^2B_2 \rightarrow {}^2E$ in D_{2d} $Cu^{II}Cl_4^{2-}$ complexes[44,45]. As a consequence of decreasing the symmetry, the ^2E state loses its degeneracy, splitting into the two close in energy states **6** and **7**. The first four excited terms corresponding to ligand field transitions are binding along the bond coordinate. An analysis of the molecular orbitals involved in the transitions to LMCT states **5-8** shows that these states mix in the region corresponding to Cu-Cl distances equal to 2.7-3.3 Å. All states situated above 20000 cm^{-1} are dissociative along the Cu-Cl bond. The states **5**, **6** and **7** degenerate from the Cu-Cl distance equal to 3.3 Å due to the formation of planar $Cu^ICl_3^{2-}$ with C_{3h} point group symmetry.

Calculated geometry and electronic spectra of $[(C_3H_7)_4N^+]_2[CuCl_4^{2-}]$ are close to the corresponding calculated parameters of the $(NMe_4)_2CuCl_4$ complex. Geometry optimization of the sixth excited state leads to the stretching of the Cu-Cl bond and the detachment of a chlorine atom (Figure 6) with the formation of $Cu^ICl_3^{2-}$. The energy of the excited state with a Cu-Cl distance equal to 4.77 Å is close to the sum of energies of the isolated species $[(C_3H_7)_4N^+]_2[Cu^ICl_3^{2-}]$ and $Cl^{\bullet}$. The geometry of the $Cu^ICl_3^{2-}$ fragment on the last steps of the excited state optimization is similar to the geometry of $Cu^ICl_3^{2-}$ anion (see Fig.6).

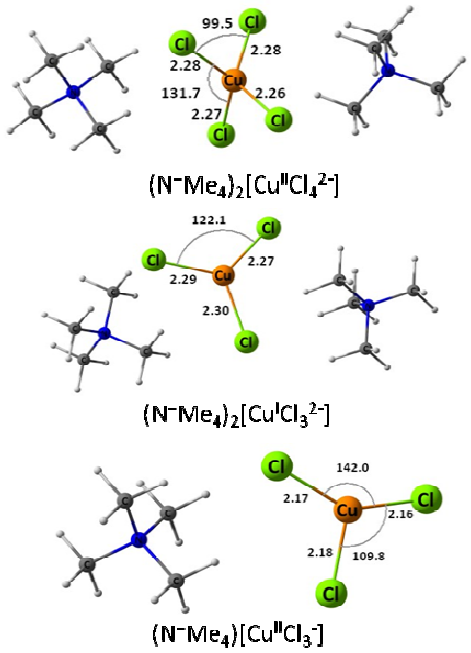

Figure 4. Optimized structures of copper chlorocomplexes with selected geometry parameters.

Discussion

A low quantum yield of the steady state photoreduction of $[(C_6H_{13})_4N]_2CuCl_4$ in solution at room temperature indicates that the major direction of phototransformations from electronic excited state **6**,**7** is the relaxation to the ground state. This could occur as a direct, radiationless relaxation to the ground state or as internal conversion *via* low-lying ligand field states. In the second case, one could observe excited state absorption (ESA) from these ligand field states in the electronic spectra. Importantly, the same ESA spectra have been detected upon excitation of $CuCl_4^{2-}$ to LF states[46]. Moreover, similar ESA of LF states at LMCT excitation of blue copper protein plastocyanin have also been observed.[47] Our results are also in agreement with this scheme. We note that after excitation of $[(C_6H_{13})_4N]_2CuCl_4$ to the second LMCT state (state **6** and **7**), internal conversion to high vibration levels of LF states may occur. This process can also result in broad absorption band in the visible region. Vibrational relaxation to the zero vibrational level of the LF state leads to a

fast reshaping of the transient absorption spectra. Two bands, at 480 nm (~20800 cm^{-1}) and 590 nm (~16900 cm^{-1}), may correspond to ESA from LF states. Indeed, the same spectra were registered after pump probe $CuCl_4^{2-}$ excitations directly to LF states[46].

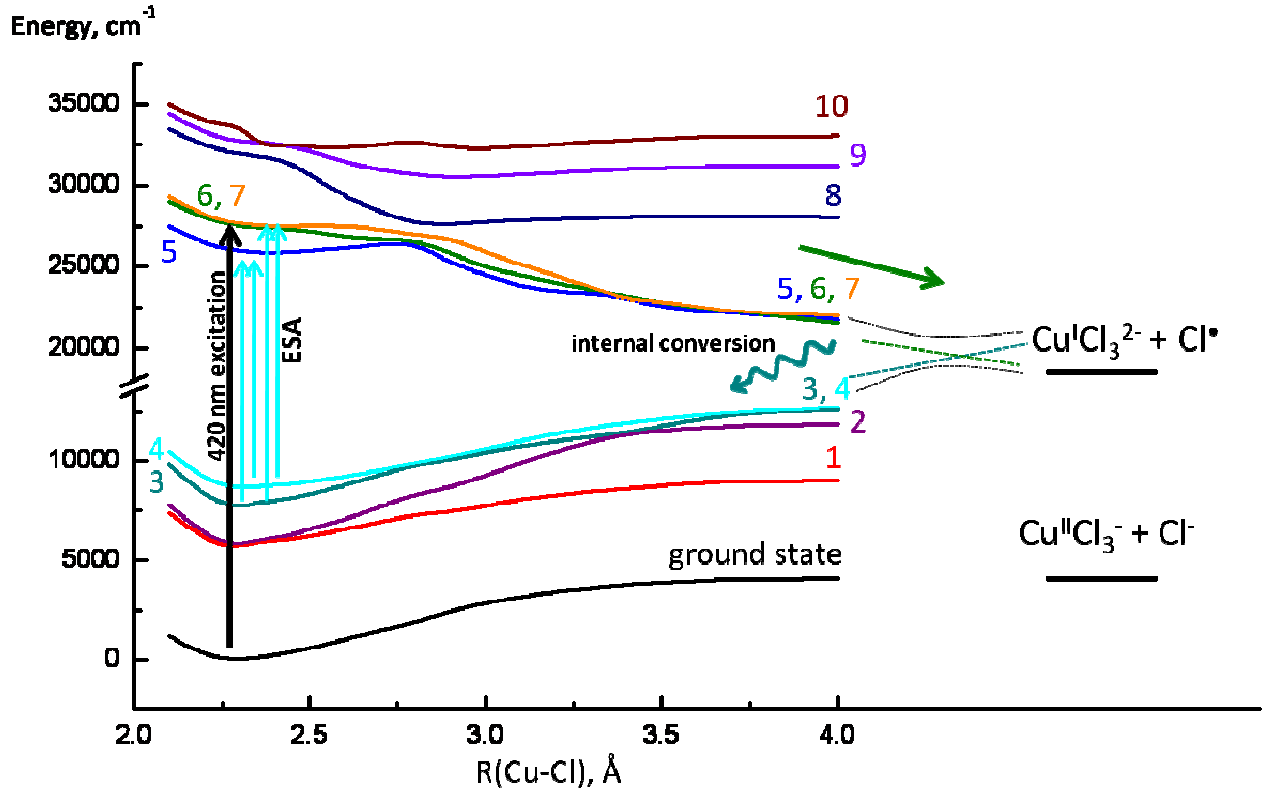

Figure 5. Electronic excited terms along Cu-Cl bond in $(NMe_4)_2CuCl_4$. Solid color lines correspond to calculated terms using TDDFT approach. Dash lines correspond to possible terms and its crossing. Full summarized energies of $Me_4N^+CuCl_3^-$ + $(CH_3)_4N^+Cl$ and $(Me_4N)_2^+CuCl_3^{2-}$ + $Cl^•$ are showed

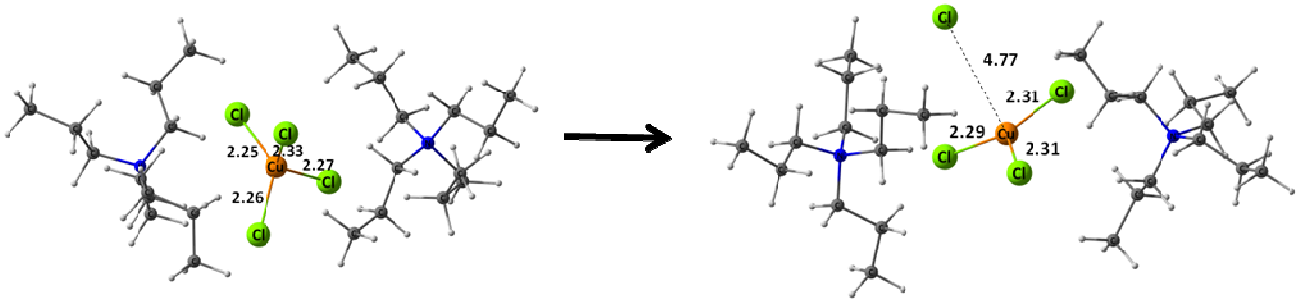

Figure 6. Optimization of sixth excited state of $[(C_3H_7)_4N^+]_2[CuCl_4^{2-}]$ complex using TDDFT approach.

The internal conversion to the LF state occurs through the crossing of LF and LMCT states. We suggest that such a crossing could exist along the Cu-Cl coordinate. In Fig. 5, the possible crossing is shown by dashed lines, whereas the directions of the photoprocesses are indicated with arrows. After excitation to states **6** and **7**, the system oscillates and falls into the crossing, which may lead to formation of the products ($CuCl_3^{2-}$ and $Cl^•$) or to conversion to high vibration levels of the LF state. All LF states are close to each other in energy. Therefore, any LF state can become populated. ESA may be observed from each LF state, according to the selection rules. For example, our quantum-chemical calculations of ESA of the highest LF state predict peaks at ~21900 and at 17200 cm^{-1}, which are close to the observed absorption bands.

Thus, on the basis of global fitting of transient spectra and kinetic traces, quantum chemical calculations of excited states, and literature data,[46] the following scheme for the irreversible, intramolecular relaxation of the $CuCl_4^{2-}$ excited state can be proposed:

Scheme 1.

We note that the states LF_1, LF_2 and LF_3 could not be attributed to distinct excited states due to these states being very close in energy. Furthermore, one cannot exclude some parallel transitions from LMST to several LF states, which are not taken into account in Scheme 1.

After relaxation to the zero vibrational level of LF states, the $CuCl_4^{2-}$ species may relax directly to the ground state without chemical transformations.

Results of quantum-chemical calculations of electronic excited terms may be used to confirm the mechanism of $CuCl_4^{2-}$ photoreduction. TDDFT calculations show that excitation to the states **6** and **7** may lead to a dissociation of $CuCl_4^{2-}$ complex accompanied by charge transfer from the chlorine anion to the copper cation with formation of a copper(I) chloro complex, $Cu^{I}Cl_3^{2-}$, and chlorine atom $Cl^{\bullet}$. The sum of the energies of isolated particles $(NMe_4)_2CuCl_3$ and $Cl^{\bullet}$ is 18500 cm^{-1} higher than the energy of $(NMe_4)_2CuCl_4$ and is close to the dissociation energy of the excited states **5**, **6** and **7**. The calculation for the sixth excited state of the $[(C_3H_7)_4N^+]_2[CuCl_4^{2-}]$ complex also predict the detachment of a chlorine atom (Figure 6). Another mechanism, which assumes outer-sphere electron transfer from solvent molecule, could occur only in the presence of donor agents with low redox potential. We expressly choose solvents and counter ions with low donor ability to make this mechanism unlikely. According to results of quantum-chemical calculations and experiment conditions, the inner-sphere electron transfer mechanism appears to be most likely. We do not observe any features corresponding to secondary thermal reactions which also may lead to formation of organocuprates in pulsed pump-probe photolysis of $[(C_6H_{13})_4N]_2CuCl_4$. The latter was found by steady state photolysis in frozen matrices. One of the reasons for the absence of thermal reactions in our study may be the low quantum yield of photoreduction ($\sim 10^{-2}$) determined by steady state photolysis. Moreover, organic radicals which may be formed in a reaction of chlorine atoms with solvent or alkyl fragments of the counter ions do not have specific absorptions in visible region.

Conclusions

The excitation of $CuCl_4^{2-}$ to LMCT states **6** and **7** result in irreversible intramolecular relaxation via three transient states (LF_1, LF_2, LF_3), or in inner-sphere photoreduction with formation of copper(I) chlorocomplex $Cu^{I}Cl_3^{2-}$ and chlorine atom.

Acknowledgments

The research was partially supported by RFBR Grants 13-03-00420a and 12-03-33104mol_a_ved. Calculations were performed using resources of Supercomputing Center of Lomonosov Moscow State University[48].

Notes and references

[a] *1-3,Leninskie gory ,Moscow, Russia. Fax: 7-495-9328846; Tel: 7-495-9391012; E-mail: legol@mail.ru (E.N.G.), kate_zub@mail.ru(E.M.Z.)*

[b] *4,Kosygina str., Moscow, Russia.; Moscow Intitute of Physics and Technology State University9 Institutskiy per., Dolgoprudny, Moscow Region, 141700, Russian Federation E-mail: nadtochenko@gmail.com*

† Electronic Supplementary Information (ESI) available. See DOI: 10.1039/b000000x/

1. E. I. Solomon, D. E. Heppner, E. M. Johnston, J. W. Ginsbach, J. Cirera, M. Qayyum, M. T. Kieber-Emmons, C. H. Kjaergaard, R. G. Hadt and L. Tian, *Chem. Rev.*, 2014, **114**, 3659-3853.
2. A. J. Clark, *Chem. Soc. Rev.*, 2002, **31**, 1–11.
3. M. J. W. Taylor, W. T. Eckenhoff and T. Pintauer, *Dalton Trans.*, 2010, **39**, 11475-11482.
4. E. I. Solomon, *Inorg. Chem.*, 2006, **45**, 8012-8025.
5. J. K. Kochi, *J. Am. Chem. Soc.*, 1962, **84**, 2121-2127.
6. P. A. C. d. Silva and P. G. David, *Bull. Chem. Soc. Jpn.*, 1982, **55**, 2673-2674.
7. A. S. Mereshchenko, S. K. Pal, K. E. Karabaeva, P. Z. El-Khoury and A. N. Tarnovsky, *J. Phys. Chem. A*, 2011, **116**, 2791-2799.
8. H. Kaczmarek, A. Kamińska, L. Å. Lindén and J. F. Rabek, *Polymer*, 1996, **37**, 4061-4068.
9. V.F. Plyusnin, N.M. Bazhin, O.B. Kiseleva, *Zh. Khim. Fiz.,* 1980, **54**, 672-675 (in Russian).
10. V.F. Plyusnin, N.M. Bazhin, O.M. Usov, *Zh. Fiz. Khim.,* 1979, **53**, 2679-2679 (in Russian).
11. E. N. Golubeva, A. V. Lobanov and A. I. Kokorin, *Russ. J. Phys. Chem. B*, 2009, **3**, 179-184.
12. E. N. Golubeva, A. V. Lobanov, V. I. Pergushov, N. A. Chumakova and A. I. Kokorin, *Dokl Chem.*, 2008, **421**, 171-174.
13. A. V. Lobanov, E. N. Golubeva, E. M. Zubanova and M. Ya. Mel'nikov, *High Energy Chem.*, 2009, **43**, 384-390.
14. E.N. Golubeva, O.I. Gromov and G.M. Zhidomirov, *J. Phys. Chem. A*, 2011, **115**, 8147–8154.
15. O. I. Gromov, E. M. Zubanova, E. N. Golubeva, V. F. Plyusnin, G. M. Zhidomirov and M. Ya. Melnikov, *J. Phys. Chem. A*, 2012, **116**, 11581-11585.
16. G. Ferraudi, *Inorg. Chem.*, 1978, **17**, 2506-2508.
17. H. Cohen and D. Meyerstein, *Inorg. Chem.*, 1986, **25**, 1505-1506.
18. N. Navon, G. Golub, H. Cohen and D. Meyerstein, *Organometallics*, 1995, **14**, 5670-5676.
19. M. Freiberg, W. A. Mulac, K. H. Schmidt and D. Meyerstein, *J. Chem. Soc. Faraday Trans.*, 1980, **76**, 1838-1848.
20. E. Baumgartner, S. Ronco and G. Ferraudi, *Inorg. Chem.*, 1990, **29**, 4747-4750.
21. S. Das and G. Ferraudi, *Inorg. Chem.*, 1986, **25**, 1066-1068.
22. A. Burg and D. Meyerstein, in *Advances in Inorganic Chemistry*, eds. E. Rudi van and I.-B. Ivana, Academic Press, 2012, vol. 64, pp. 219-261.
23. W. T. Eckenhoff and T. Pintauer, *Catal. Rev.*, 2010, **52**, 1-59..
24. W. A. Braunecker and K. Matyjaszewski, *Prog. Polym. Sci.*, 2007, **32**, 93-146.
25. E. N. Golubeva, D. N. Kharitonov, D. I. Kochubey, V. N. Ikorskii, V. V. Kriventsov, A. I. Kokorin, J. Stoetsner and D. W. Bahnemann, *J. Phys. Chem. A*, 2009, **113**, 10219-10223.
26. A. Kh. Vorobiev and N. A. Chumakova *in Nitroxides - Theory, Experiment and Applications*, Ed. A.I. Kokorin (Ed.), InTech, 2012.
27. I. V. Shelaev, F. E. Gostev, M. I. Vishnev, A. Y. Shkuropatov, V. V. Ptushenko, M. D. Mamedov, O. M. Sarkisov, V. A. Nadtochenko, A. Y. Semenov and V. A. Shuvalov, *J. Photochem. Photobiol.*, 2011, **104**, 44-50.
28. S. A. Kovalenko, A. L. Dobryakov, J. Ruthmann and N. P. Ernsting, *Phys. Rev. A*, 1999, **59**, 2369-2384.
29. F. Neese, *WIREs Comput. Mol. Sci.*, 2012, **2**, 73-78
30. R. K. Szilagyi, M. Metz and E. I. Solomon, *J. Phys. Chem. A*, 2002, **106**, 2994-3007.
31. A. Schaefer, H. Horn and R. Ahlrichs, *J. Chem. Phys.*, 1992, **97**, 2571-2577.
32. D.E. Woon and T.H. Dunning, Jr. *J. Chem. Phys.,* 1993, **98**, 1358-1371.

33. S. Sinnecker, A. Rajendran, A. Klamt, M. Diedenhofen and F. Neese, *J. Phys. Chem. A*, 2006, **110**, 2235-2245.
34. T. Petrenko, S. Kossmann and F. Neese, *J. Chem. Phys.*, 2011, **134**, 054116.
35. F. Neese, F. Wennmohs, A. Hansen and U. Becker, *Chem. Phys.*, 2009, **356**, 98-109.
36. W. H. Moore and S. Krimm, *Spectrochim. Acta A ,* 1973, **29**, 2025-2042.
37. W. H. Moore, J. H. C. Ching, A. V. R. Warrier and S. Krimm, *Spectrochim. Acta A*, 1973, **29**, 1847-1858.
38. A. N. Kostrov, A. V. Aybushev, F. E. Gostev, I. V. Shelayev, O. M. Sarkisov, N. N. Denisov, D. V. Khudyakov and V. A. Nadtochenko, *High Energy Chem.*, 2011, **45**, 250-257
39. P. Kukura, D. W. McCamant and R. A. Mathies, *Annu. Rev. Phys. Chem.*, 2007, **58**, 461-488.
40. Y. Suffren, F.-G. Rollet and C. Reber, *Comments Inorg. Chem.*, 2011, **32**, 246-276
41. E. R. Henry, *Biophys. J.*, 1997, **72**, 652-673.
42. N. P. Ernsting, S. A. Kovalenko, T. Senyushkina, J. Saam and V. Farztdinov, *J. Phys. Chem. A*, 2001, **105**, 3443-3453.
43. R. Clay, J. Murray-Rust and P. Murray-Rust, *Acta Crystallographica Section B*, 1975, **31**, 289-290
44. J. Ferguson, *J. Chem. Phys.*, 1964, **40**, 3406-3410
45. M. Ehara, P. Piecuch, J. J. Lutz and J. R. Gour, *Chem. Phys.*, 2012, **399**, 94-110
46. A. S. Mereshchenko, Ph.D. Dissertation. Graduate College of Bowling Green State University: USA, 2013.
47. M. D. Edington, W. M. Diffey, W. J. Doria, R. E. Riter and W. F. Beck, *Chem. Phys. Lett.*, 1997, **275**, 119-126.
48. V. Sadovnichy, A. Tikhonravov, Vl. Voevodin, and V. Opanasenko "Lomonosov": Supercomputing at Moscow State University. In *Contemporary High Performance Computing: From Petascale toward Exascale* (Chapman & Hall/CRC Computational Science), pp.283-307, Boca Raton, USA, CRC Press, 2013.

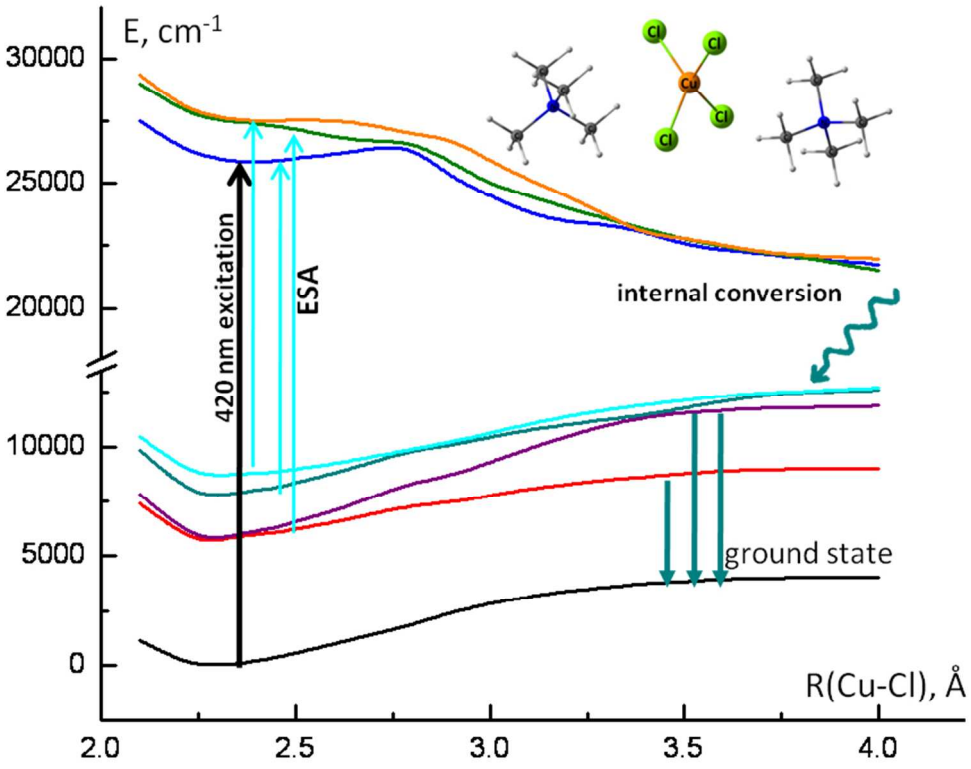

149x121mm (150 x 150 DPI)